

This discussion paper is/has been under review for the journal Biogeosciences (BG).  
Please refer to the corresponding final paper in BG if available.

# A survey of carbon monoxide and non-methane hydrocarbons in the Arctic Ocean during summer 2010: assessment of the role of phytoplankton

S. Tran<sup>1</sup>, B. Bonsang<sup>1</sup>, V. Gros<sup>1</sup>, I. Peeken<sup>2,3</sup>, R. Sarda-Estevé<sup>1</sup>, A. Bernhardt<sup>2</sup>, and S. Belviso<sup>1</sup>

<sup>1</sup>Laboratoire des Sciences du Climat et de l'Environnement, UMR8212, CEA/CNRS/UVSQ – CE Saclay, Bat. 701 Orme des Merisiers, 91191, Gif-Sur-Yvette, France

<sup>2</sup>Alfred Wegener Institute for Polar and Marine Research (AWI), Biological Oceanography, Am Handelshafen 12, 27570, Bremerhaven, Germany

<sup>3</sup>Center for Marine Environmental Sciences (MARUM), Leobener Strasse, 28359 Bremen, Germany

Received: 5 March 2012 – Accepted: 14 March 2012 – Published: 18 April 2012

Correspondence to: B. Bonsang (bernard.bonsang@lsce.ipsl.fr)

Published by Copernicus Publications on behalf of the European Geosciences Union.

4727

## Abstract

During the ARK XXV 1+2 expedition in the Arctic Ocean carried out in June–July 2010 aboard the R/V *Polarstern*, we measured carbon monoxide (CO), non-methane hydrocarbons (NMHC) and phytoplankton pigments at the sea surface and down to a depth of 100 m. The CO and NMHC sea-surface concentrations were highly variable; CO, propene and isoprene levels ranged from 0.6 to 17.5 nmol l<sup>-1</sup>, 1 to 322 pmol l<sup>-1</sup> and 1 to 541 pmol l<sup>-1</sup>, respectively. The CO and alkene concentrations were enhanced in polar waters off of Greenland, which were more stratified because of ice melting and richer in chromophoric dissolved organic matter (CDOM) than typical North Atlantic waters. The spatial distribution of the surface concentrations of CO was consistent with our current understanding of CO-induced UV photo-production in the sea. The vertical distributions of the CO and alkenes followed the trend of light penetration, with the concentrations displaying a relatively regular exponential decrease down to non-measurable values below 50 m. However, no diurnal variations of CO or alkene concentrations were observed in the stratified and irradiated surface layers. This finding suggests that the production and removal processes of CO and alkenes were tightly coupled. We tentatively determined a first-order rate constant for the microbial consumption of CO of 0.5 d<sup>-1</sup>, which is in agreement with previous studies. On several occasions, we observed the existence of subsurface CO maxima at the level of the deep chlorophyll maximum. This finding represents field evidence for the existence of a non-photochemical CO production pathway, most likely of phytoplanktonic origin. The corresponding production rates normalized to the chlorophyll content were in the range of those estimated from laboratory experiments. In general, the vertical distributions of isoprene followed that of the phytoplankton biomass. Hence, oceanic data support the existence of biological production of CO and isoprene in the Arctic Ocean.

4728

## 1 Introduction

Carbon monoxide (CO) and non-methane hydrocarbons (NMHC) are ubiquitous in the remote marine troposphere and play a key role in determining the oxidizing capacity of Earth's atmosphere (Thompson, 1992; Prather et al., 2001). These compounds are major consumers of OH radicals and are strongly involved in lowering levels of this dominant atmospheric oxidant in the remote marine atmosphere. The lifetime of tropospheric CO is approximately 2 months (Crutzen, 1994; Prather, 1996), while the NMHC lifetimes range from a few hours up to several days (Logan et al., 1981; Atkinson, 1990). Isoprene has long been recognized as the dominant NMHC produced (Rasmussen and Went, 1965; Zimmerman et al., 1988). While terrestrial vegetation is the main source of isoprene, it has been shown that productive oceanic areas can emit isoprene at rates that can potentially influence the budget of reactive trace gases and oxidants in the remote atmosphere (Bonsang et al., 1992; Broadgate et al., 1997; Ayers et al., 1997; Lewis et al., 1997, 2001; Carslaw et al., 1999; Liakakou et al., 2007). In addition to its photochemical role, isoprene is also a precursor of secondary organic aerosols over continental areas (Kanakidou et al., 2005 and references therein; Kroll and Seinfeld, 2008) and, possibly to a lesser extent, over the oceans (Arnold et al., 2009; Gant et al., 2010).

Surveys of CO (Swinerton and Lamontagne, 1974; Stubbins et al., 2006; Xie et al., 2009) and NMHC concentrations (Rudolph and Ehhalt, 1981; Bonsang et al., 1988, 1992; Milne et al., 1995) in the ocean and the remote marine atmosphere have shown that the surface ocean is generally a source of reactive CO and NMHC because it is supersaturated with respect to the atmosphere. Estimates of the global marine emissions of CO span a large range from 3 to 600 Tg C yr<sup>-1</sup> (Bates et al., 1995; Zuo and Jones, 1995; Rhee, 2000). The results of more recent assessments are contrasting: Stubbins et al. (2006) provided rather low fluxes ( $3.7 \pm 2.6$  Tg C yr<sup>-1</sup>), and using a model of CO photoproduction in the euphotic layer, Fichot et al. (2010) predicted a global marine source of CO of 41 Tg C yr<sup>-1</sup>. The global marine emissions of NMHC are estimated

4729

to range between 2 and 50 Tg C yr<sup>-1</sup>. These emissions were obtained from regional measurements extrapolated to the global scale (Bonsang et al., 1988; Guenther et al., 1995; Plass-Dulmer et al., 1995; Ratte et al., 1998). For example, the value of 2 Tg C yr<sup>-1</sup> provided by Plass-Dulmer et al. (1995) was based on measurements conducted only in oligotrophic waters. The marine source of isoprene is estimated to range between 0.31 and 1.09 Tg C yr<sup>-1</sup>. These values are quite small compared to the estimated global emissions of isoprene of ~400–750 Tg C yr<sup>-1</sup> (Guenther et al., 2006; Müller et al., 2008).

Marine CO and NMHC are hypothesized to be produced mainly photochemically from the interactions between UV-light and chromophoric dissolved organic matter (CDOM). In accordance, dissolved CO concentrations can display strong diurnal variations, with maxima in the early afternoon and minima at dawn (Swinerton et al., 1970; Conrad et al., 1982; Jones, 1991; Bates et al., 1995; Zafiriou et al., 2008). The photochemical production of CO (Kettle, 2005; Zafiriou et al., 2008; Xie et al., 2009) is better understood than that of NMHC (Lee and Baker, 1992; Ratte et al., 1993, 1998; Riemer et al., 2000). The production depends on the UV-absorption coefficient of CDOM in the water column and the CO quantum yield, which are both wavelength dependent and relatively well parameterized (Kettle, 2005; Fichot and Miller, 2010). Additionally, biological production of CO has been recently observed in laboratory experiments, but the production pathways remain unclear (Gros et al., 2009). To date, there was no evidence for the biological production of CO from field observations. Conversely, isoprene is known to be produced biologically (Bonsang et al., 1992, 2010; Shaw et al., 2003, 2010; Milne et al., 2005; Arnold et al., 2009), making it interesting to investigate the spatial and temporal variation of CO and isoprene concomitantly. The main sinks of oceanic CO are air-sea gas exchange and microbial oxidation (Zafiriou et al., 2003), while air-sea gas exchange is the only known sink for NMHC (Palmer and Shaw, 2005). Evidence for the microbial consumption of NMHC, including isoprene, is lacking.

In polar regions, which are the most sensitive areas to the effects of global warming, only a few researchers have reported oceanic CO and NMHC measurements

4730











concentrations at the surface were in the range from undetectable values to several hundreds of  $\text{pmol l}^{-1}$ . The dominant class of light hydrocarbons was alkenes. The lowest levels of CO and propene were  $0.6 \text{ nmol l}^{-1}$  and  $1 \text{ pmol l}^{-1}$ , respectively.

The wide range of variability in CO and propene concentrations is shown in the contour plots presented in Fig. 4, together with the distributions of CDOM. The CDOM levels were higher in the pack ice along the Greenland coast where CO and alkene levels were enhanced. In particular, hot spots of CO and propene concentrations occurred on the N-S transect between  $76$  and  $78^\circ \text{N}$ . Another hot spot of CO concentration occurred close to Jan Mayen Island, but unfortunately, no alkene measurements were conducted in this region. Similarly, low concentrations of CO and propene were simultaneously observed when low concentrations of CDOM occurred.

## 4.2 Variations along the 4 sections

Each of the following plots displays the surface concentrations of CO and propene, sea-surface temperature, CDOM levels, global solar radiation, latitude, wind speed and bathymetry. Note that there are gaps in the records for several reasons, including the shift from surface sampling to vertical sampling, instrument calibration or instrument failure.

Section one (Fig. 5) covered a large latitudinal range from the Norwegian coasts to Greenland and crossed the Norwegian Basin (cf. bathymetry Fig. 5d). The surface-seawater CO concentration ranged from  $1.0$  to  $11.7 \text{ nmol l}^{-1}$ , with a mean value of  $4.3 \pm 2.1 \text{ nmol l}^{-1}$  (Fig. 5a). The average propene concentration was  $89 \pm 58 \text{ pmol l}^{-1}$ . There was no clear correspondence between CO and propene. The sea-surface temperature decreased towards the north from  $11^\circ \text{C}$  to  $-0.6^\circ \text{C}$ . There was a clear transition from Atlantic Water (AW) masses to PW (Fig. 5b). A front was crossed while approaching Jan Mayen Island, characterized by a temperature drop of  $3^\circ \text{C}$  associated with a change of water masses from WAW to FAW. CDOM values were low all along this section (below  $0.5$  arbitrary units) but increased slightly on the Greenland shelf. The sunniest days were observed at the beginning of the transect (Fig. 5c),

4741

during which the total radiation reached  $900 \text{ W m}^{-2}$ , while on the other days, the maximum radiation was below  $600 \text{ W m}^{-2}$ . There was a decreasing trend in wind speed (Fig. 5d) from  $25 \text{ m s}^{-1}$  at the beginning of the section to  $3 \text{ m s}^{-1}$  by the end. Only two vertical profiles were recorded, one close to Jan Mayen Island and the second along the Greenland coast.

Section two (Fig. C1 shown in Appendix C) crossed the Greenland Basin roughly at  $75^\circ \text{N}$ . The surface-seawater CO concentration ranged from  $0.5$  to  $10.5 \text{ nmol l}^{-1}$ , with a mean CO value of  $4.3 \pm 2.6 \text{ nmol l}^{-1}$ . The propene concentrations were quite low (in the range of  $1$  to  $72 \text{ pmol l}^{-1}$ ) but showed the same pattern as CO. The average concentration of propene was  $23 \pm 14 \text{ pmol l}^{-1}$ . The transect stations included FAW water masses with an average SST of  $2.8 \pm 0.4^\circ \text{C}$  and constant low CDOM values. At the end of the transect and during a short route toward the north, WAW water masses were encountered. Nine stations were sampled during the transect at  $75^\circ \text{N}$ .

Section 3 (Fig. C2 in Appendix C) covered the entire Fram Strait from east to west. The ship sometimes travelled north to reach the HAUSGARTEN area of investigation. The sampling from this section lasted 23 days. A total of 22 stations were investigated. The CO values ranged from  $1.0$  to  $14.4 \text{ nmol l}^{-1}$ , with a mean surface CO concentration of  $3.8 \pm 2.6 \text{ nmol l}^{-1}$ . The propene concentration ranged from  $2$  to  $303 \text{ pmol l}^{-1}$ , with an average value of  $87 \pm 44 \text{ pmol l}^{-1}$ . During this section, the ship crossed four different water masses (PW, AW, FAW and WAW), with sharp changes of the sea-surface temperature (up to  $7^\circ \text{C}$ ) while meeting PW. The CDOM values increased 5-fold at the end of this section. It appears that the CO concentrations were much more influenced by the presence of polar waters than by irradiance.

The last section (Fig. 7) on the way back from the Greenland coast to Iceland lasted 3 days. Pack ice was present over the Greenland shelf. The polar waters were associated with the East Greenland Current and had high CDOM levels (Fig. 7b). The CO and propene concentrations ranged from  $1.1$  to  $17.5 \text{ nmol l}^{-1}$  and  $45$  to  $322 \text{ pmol l}^{-1}$ , respectively. High CO concentrations (mean value of  $5.9 \pm 4.9 \text{ nmol l}^{-1}$ ) up to  $17.5 \text{ nmol l}^{-1}$  and high propene concentrations (average of  $235 \pm 29 \text{ pmol l}^{-1}$ )

4742



were observed from 23 to 25 July (Fig. 7a). The influences of the bathymetry and pack ice on the CO concentrations are obvious (Fig. 7d). The CO and propene concentrations showed the same trend except for the night of 25 July, when the CO concentration began to decrease, while the propene values remained high. Off of Jan Mayen Island (Fig. 7d), in AW, a peak of CO concentration was measured ( $17.5 \text{ nmol l}^{-1}$ ). Unfortunately, the propene concentrations were not measured, and the solar-radiation and wind-speed sensors were switched off from 26 July in the morning (Fig. 7c, d).

In general, it appears that CO and NMHC concentrations are consistent with surface-seawater temperature (Figs. 5 to 7). Specifically, between 7 to 9 July (Fig. 6) and from 24 to 25 July (Fig. 7), temperature drops of 5 to 7 degrees are associated with a simultaneous increase of CO and propene concentrations. On average, polar waters, which are characterized by low temperature ( $<5^\circ\text{C}$ ) and salinity ( $<34.7$ ), are enhanced in CO and propene (alkenes), with mean concentrations of  $6.5 \text{ nmol l}^{-1}$  and  $125 \text{ pmol l}^{-1}$ , respectively (Table 4), whereas FAW or WAW contained 2-fold lower concentrations. It is particularly interesting that isoprene displays an opposite trend, with concentrations significantly higher in warm waters than in polar waters.

### 4.3 Vertical distributions of CO and NMHC concentrations

All of the vertical profiles were first plotted together and averaged, and the mean depth profiles of CO and light alkenes down to a depth of 100 m are displayed in Fig. 8. The concentrations show a regular decrease with depth comparable to that of light penetration (PAR, Fig. 8 and UVA, Fig. 10). In the case of isoprene, its vertical distribution is more consistent with the chlorophyll *a* distribution than with the profile of the light-penetration curve (Fig. 9) and is characterized by a systematic subsurface maximum between 10 and 30 m depth.

The stations s237 and s194, located in polar waters with significant sea-ice coverage and in open water, respectively, had the highest concentrations of CO and propene at the surface. The other stations showed the same pattern to a lesser extent, which will be discussed in Sect. 5.3. Polar waters (typical ice station: station 237) showed

4743

the highest gas concentrations in the mixed layer (0 to 15 m depth for station 237) combined with a steep decrease of concentration with depth. In contrast, in open-water stations (e.g. station 194), the decreases of CO and propene concentrations with depth were spread throughout the upper 40 m layer, while the mixed layer was limited to 0 to 8 m of depth for station 194. As shown above, the vertical distributions of CO and propene are clearly influenced by the light profile. However, the vertical gradients of CO and propene appear steeper in polar waters.

## 5 Discussion

For dissolved carbon monoxide, our results are comparable to other measurements of surface water in the Arctic Ocean, particularly with the first measurements by Swinerton and Lamontagne (1974), who report an average concentration of  $2.5 \text{ nmol l}^{-1}$ . Recently, the CO concentration measured in the Beaufort Sea (during spring) ranged from  $0.98$  to  $13 \text{ nmol l}^{-1}$ , with a mean value of  $4.72 \pm 2.42 \text{ nmol l}^{-1}$  (Xie et al., 2009). For other oceanic areas, the surface-seawater CO concentrations are in the range of  $0.4$  to  $2.6 \text{ nmol l}^{-1}$  over the Atlantic Ocean (Stubbins et al., 2006) and  $0$  to  $5.8 \text{ nmol l}^{-1}$  over the Pacific Ocean (Bates et al., 1995). The values reported here were thus of the same order of magnitude. Nevertheless, the maximal values found in the Arctic Ocean were the highest among the previously reported CO measurements in the open ocean. For NMHC, our results are also in agreement with the previous data reported in the literature (Plass-Dülmer et al., 1995), but because no specific investigations of NMHC were performed in arctic regions, a direct comparison with previous data cannot be made.

The mean vertical profiles of CO and selected NMHC concentrations measured in the upper 100 m of the ocean throughout the entire campaign showed that the concentrations of those compounds in the water column gradually decreased with depth (Fig. 8a and b), as reported in many other studies (Conrad et al., 1982; Johnson and Bates, 1996; Ohta, 1997; Kettle, 2005; Day and Faloon, 2009; Yang et al., 2011). This

trend was characterized by a quasi-exponential decrease with a variable e-fold value of a few meters (for PW) to 15–20 m for AW, attributed to the rapid attenuation of the actinic flux available for CDOM photolysis. The highest CO concentration at each station was always observed at the sea surface and then decreased rapidly in the top 100 m layer. The variation patterns of CO concentration were comparable to those of photosynthetically active radiation (PAR) (Fig. 8c) and UVA penetration, indicating that the production at different depths was principally driven by the decrease of light intensity. In the absence of mixing, the CO profile would be expected to roughly coincide with that of UV penetration, according to other reports (Zafiriou, et al., 2003; Kettle, 2005; Xie et al., 2009).

Because the mean propene depth profile (Fig. 8b) presented the same pattern, a similar mechanism of production can be assumed, as already suggested by Ratte et al. (1998). Our results were thus in agreement with other studies and confirmed that CO and alkene concentrations have very similar production mechanisms in the euphotic zone, mainly driven by light (UV) penetration.

The alkane concentrations seemed to be well mixed in the water column and did not show any significant variability (profiles not shown here). Ratte et al. (1998) investigated alkane measurements in seawater and described similar features. The authors concluded that alkane concentrations generally exhibited irregular fluctuations, and thus the factors determining alkane concentrations were different from those for propene and isoprene.

Many authors have already reported this deep-maximum pattern for isoprene concentration profiles (Bonsang et al., 1992; Milne et al., 1995), which was similar to that of phytoplankton productivity in terms of chlorophyll *a* concentration.

Our results demonstrate the importance of the different variables that influence the temporal and spatial variability of carbon monoxide or NMHC in the ocean. The surface variability of CO and NMHC and their vertical distributions in the euphotic zone depend on the combination of sources and sinks involving solar radiation, temperature, ventilation at the air-sea interface, CDOM content and phytoplankton biomass

4745

and distributions. As a first approach, our results indicate that solar radiation drives the vertical distributions of CO and alkenes, whereas phytoplankton abundance is the dominant factor explaining the vertical structure of isoprene concentrations in the euphotic zone. However, large deviations from these simple considerations are observed, particularly if we try to understand the spatial and temporal variability of trace gases in the ocean.

### 5.1 Sinks and budgets in the water column

For a better understanding of the processes governing CO and NMHC in the water column, a simple box model that includes the knowledge of the main identified sources and sinks has been established.

First, one dominant sink effect in the mixed layer is the gas exchange at the seawater interface. Several authors have also suggested microbial consumption of CO in the water column and introduced a microbial loss-rate constant derived from incubation experiments of  $0.55 \text{ d}^{-1}$  for temperate waters (Kettle, 2005) and in the range of 0.49 to  $0.69 \text{ d}^{-1}$  for arctic zones (Xie et al., 2009). Our storage experiment (discussed in the section “Sample collection and storage”) led to a loss-rate constant of CO of  $0.49 \text{ d}^{-1}$  ( $5.7 \times 10^{-6} \text{ s}^{-1}$ ), surprisingly very close to the values reported by Xie et al. (2009). This constant could therefore be attributed to microbial consumption and used in CO-budget calculations.

No microbial consumption was observed for NMHC in our experiment; furthermore, this effect has never been reported in the literature and can therefore be considered as negligible. Other sinks, such as oxidation, are most likely of minor importance (Riemer et al., 2000).

The gas exchange at the interface is one main sink for all of the measured species, according to their large supersaturation observed in surface waters. The corresponding piston velocity was calculated from the parameterization defined by Wanninkhof (1992) and based on the determination of the Schmidt number according to classical diffusivity equations (see Appendix B).

4746

The vertical transport toward deeper layers will not be considered here as a first approximation because the concentrations of the measured species fall to negligible values at the bottom of the euphotic zone, and consequently, any advection or diffusion term should be close to zero.

- 5 On the basis of these preliminary considerations, a budget evaluation could be approached from the determination of the content  $Q_{ML}$  (in  $\text{mol m}^{-2}$ ) of a given species in the water column by integrating its concentration from the surface to the depth of the mixed layer ( $Z_{ML}$ ):

$$Q_{ML} = \int_{0m}^{Z_{ML}} C_{(z)} dz = \bar{C}_{ML} Z_{ML} \quad (2)$$

- 10 In a first approximation, the different sinks can be characterized using a first-order time constant. The constant,  $k$ , for ventilation to the atmosphere is given by the following ratio:

$$k = \frac{K_w}{Z_{ML}} \quad (3)$$

- 15 With the microbial consumption parameterized using a constant coefficient  $\mu$ , the production  $P$  of a given species (possibly including various processes  $\Sigma P_{ML}$ ) in the mixed layer can therefore be derived from a steady-state equation:

$$\Sigma P_{ML} = Q_{ML} \left( \frac{K_w}{Z_{ML}} + \mu \right) = \bar{C}_{ML} Z_{ML} \left( \frac{K_w}{Z_{ML}} + \mu \right) = \bar{C}_{ML} Z_{ML} (k + \mu) \quad (4)$$

- 20 The budget can be relatively well calculated for the mixed layer, where the main sinks are clearly identified (microbial consumption and air-sea transfer for CO; air-sea transfer only for NMHC), and for the deeper layers, no significant transport occurs with the mixed layer through the pycnocline level. Budget calculations could be conducted using the same approach; however, such calculations are more difficult to establish, particularly for NMHC because no significant sink can be considered.

4747

## 5.2 Temperature and water-mass dependences

- As shown in Figs. 6 and 7 and Table 4, there was a clear link between water masses and CO/propene concentrations. Several reasons can be considered to explain the dependence of CO or NMHC surface concentrations on temperature. A first possible effect could be purely physical and due to the dependence of the air-sea exchange velocity (piston velocity) on the surface-seawater temperature, leading to a variation in the overall contribution of this sink in the budget of the water column and consequently of the residence time of CO or NMHC in the water column and of their accumulation rate. Lower temperatures associated with lower diffusivity coefficients and exchange speeds are in favor of an increase of the CO or NMHC levels due to an increase of their residence time in the surface layers.

- As a first step, we evaluated the sensitivity to surface temperature of the CO budget in the water column. The average profile of CO in water (Fig. 8a) appears to be quasi-exponential with depth, (with an exponential coefficient of  $7.5 \times 10^{-2} \text{ m}^{-1}$ ). This observation is in accordance with the fact that the production rate is governed by the absorption of UV radiation, with a relatively constant absorption coefficient in the column, mainly driven by the CDOM content. Taking into account a mixed layer of approximately 20 m, the average CO concentration in the mixed layer given by Eq. (1) is approximately  $[\text{CO}]_{\text{surface}}/2$ , which is also very close to the CO measured at 6 m depth of  $[\text{CO}]_{\text{surface}}/1.6$ .

The sinks of CO in the mixed layer include:

1. microbial consumption with a coefficient  $\mu$  experimentally determined as  $5.7 \times 10^{-6} \text{ s}^{-1}$  or  $0.49 \text{ d}^{-1}$ , and
2. the exchange at the air-sea interface characterized by a loss coefficient given by Eq. (2).

Therefore, assuming a steady state for the content of CO in the mixed layer, with a constant photoproduction term, sensitivity tests were made for a microbial consumption  $\mu$

4748

experimentally determined and surface-seawater temperature of 11.5 °C (the maximum observed during the campaign) and −1.4 °C (the minimum observed).

For this range of temperatures, we have:

$$K_{w,11.5} = 5.91 \times 10^{-5} \text{ m s}^{-1} \text{ and } K_{w,-1.35} = 3.90 \times 10^{-5} \text{ m s}^{-1} \quad (5)$$

5 This calculation leads to a  $K_w/Z_{ML}$  coefficient (Eq. 2) of  $\sim 3.0 \times 10^{-6}$  and  $\sim 2.0 \times 10^{-6} \text{ s}^{-1}$  for the maximum and minimum observed temperatures, respectively. Therefore, it can be stated that microbial consumption and air-sea exchange correspond to sinks of the same order of magnitude. The sum of these sinks, according to the range of variation of surface temperature, consequently only varies from  $8.0 \times 10^{-6}$  to  $9.0 \times 10^{-6} \text{ s}^{-1}$ , a figure that can only explain  $\sim 10\%$  of the CO variability. The physical effect of temperature is therefore of minor importance in the variability of the CO concentrations observed (2-fold variation) between WAW and PW.

15 Similar calculations can be conducted for alkenes. However, in this case, no microbial consumption is involved. The only sink in this case is the air-sea gas exchange, and the effect of temperature would be more pronounced, with a relative change in the  $K_w/Z_{ML}$  coefficient of roughly 50 % between warm and cold waters. This physical effect of temperature is still not sufficient to explain the observed concentrations, which vary more than 2-fold between WAW and PW. In summary, these considerations clearly show that the physical effect of temperature cannot explain the increase of CO and 20 alkene surface-seawater concentrations observed in the Arctic Ocean.

### 5.3 Photoproduction of CO and propene

Numerous variables were considered to explain the observed variations in the surface concentrations of CO and propene. The first obvious variable is solar radiation because in previous studies, a relation between these compounds and the diurnal cycle has been observed. The average global radiation diurnal cycle is shown in Fig. 11a. The maximum solar radiation of  $295 \pm 139 \text{ W m}^{-2}$  occurred between 12:00

4749

and 15:00 UTC, and minimum values were measured at night, with an average value of  $31 \pm 15 \text{ W m}^{-2}$ . Compared with the average diurnal cycle of CO concentration over the cruise (Fig. 11b), in which no significant diurnal cycle was detected, solar radiation seemed not to be the dominant process that explained the CO variability at the surface. Although daily surface-seawater CO measurements were not performed during the whole period (due to station sampling), the measurements did not reveal any clear diurnal signals. It seemed that light did not act directly on the CO variability. These results are in agreement with the observations of Xie et al. (2009), who found that no diurnal cycle of surface-water CO concentration occurred in spring. Similarly, the alkene surface measurements, although conducted with a reduced spatial resolution, did not show any diurnal trends.

15 The fluorescent signal of CDOM measured on board (Figs. 5b, 6b, 7b) was 5-fold greater in PW than in the other water masses. Several authors (Belzile et al., 2000; Scully and Miller, 2000) have noted the release of organic matter during ice melting due to algae growing in the ice, which might explain the generally higher values of CDOM in the ice-covered PW. An additional source of CDOM in sea ice could be the incorporation of detritus from rivers during ice development on the Siberian shelves (Nurnberg et al., 1994). The co-occurrence of CO and CDOM production in PW combined with UV radiation is known to be the main source of CO in seawater, and our observations confirmed this combination as a first-order process.

20 Fichot et al. (2010) have recently studied and simulated the global production of CO by the photo-degradation of CDOM, and Fig. 12 shows their estimates for our investigation area. Our spatial distributions of CO at the sea surface (Fig. 4a) are compared to the output of the model by Fichot et al. (2010), facilitating the comparison of the variability of our measured concentrations and their calculated production rate at the sea surface. The hot spot of measured CO along the Greenland coast was unfortunately not documented in the model (Fig. 12a). Higher production rates were found in the area of section 2 (at 75° N) and along section 4 (transect north to south) before Jan Mayen Island. The CO measurements showed high concentrations in the same

area from 75° N to 80° N, where high values of CDOM were also found. In this area, the measured CO and CDOM values fitted with the photochemical production of CO at the sea surface.

5 However, the other areas with high production rates did not match with the variability of our measurements, demonstrating the limit of comparison between the production rates calculated per day and our local measurements of concentrations at a given location. However, the model still provides a good general view of sea-surface CO fluxes over the whole Arctic.

10 The similar behavior of CO and alkenes suggests that their sources in oceanic waters have a common origin in the UV-induced photodecomposition of organic matter. This assumption can be confirmed by the comparison of their average concentrations at the surface throughout the experiment and their quantum yields  $\Phi$  (in mole of CO or alkenes produced per mole of photon in UV absorbed by CDOM) with respect to photo-production. However, because the sinks for CO and alkenes are different, we consider  
15 that their mean concentrations in the mixed layer are driven by the equilibrium between their sinks and sources (Eq. 3). These quantum yields of photo-production have been estimated on average for CO at  $1.8 \times 10^{-5}$  ( $1 \times 10^{-4}$  to  $2 \times 10^{-6}$  for wavelengths from 300 to 400 nm, Zafiriou et al., 2003) and 2 to 3 orders of magnitude lower for propene, isobutene and 1-butene (Table 5, Riemer et al., 2000). On the basis of Eqs. (2) and (3)  
20 with a hypothesized common photochemical source (i.e. production proportional to the quantum yield), we should have a constant ratio ( $R$ ) for CO and alkenes:

$$\frac{\overline{C_{ML}}(k + \mu)}{\Phi} = R \quad (6)$$

The results are presented in Table 5 for the mean conditions of temperature and wind speed measured for the vertical profiles. The results show that the ratio given by Eq. (4)  
25 is very close for CO and alkenes and that the hypothesis of a common photoproduction process for CO and alkenes is consistent with our knowledge of the magnitude of their sources and sinks.

4751

However, in addition to these common fates characterizing the vertical profiles of CO and alkenes, great variability was observed in the absolute concentrations, with the surface concentration roughly reflecting the variability in depth and the contents of the water column. Two main differences can be found between our profiles and  
5 the simulations of Fichot et al. (2010). First, we still find significant CO concentrations at 20 m depth, while the model of Fichot et al. (2010) showed very low or even no photo-production of CO (Fig. 12b) at this depth in the same study area. A second main difference is the occurrence of relative high secondary deep CO concentrations, which were usually observed close to the chlorophyll maximum (purple dots in Fig. 1).

10 Because Fichot et al. (2010) showed that there was no photo-production from CO at 20 m depth, the deviation of the CO standard profile should be due to a previously unconsidered variable.

We have until now taken into account only simple physical or chemical parameters to understand the CO and NMHC distributions in the upper layer of seawater. However,  
15 this approach failed to explain all of the observed variability, and it is therefore necessary to take into account the role of biology for a better understanding of the evolution of trace gases in the studied environment.

#### 5.4 Influence of biology on trace gas production

The comparison of our data as displayed in Fig. 4 with the modeling results of Fichot  
20 et al. (2010, Fig. 12) suggests that CDOM was not the only variable that influenced CO concentration. Indeed, the levels of chlorophyll *a* in seawater seem to also drive some events of high CO concentrations, as on 19 and 26 July. Figure 13 shows, for example, that high concentration of CO aligned with an increase of chlorophyll *a* concentrations, while CDOM concentration was low. This observation was consistent with the study of  
25 Gros et al. (2009), who performed laboratory experiments with phytoplankton and have suggested that CO was produced directly from phytoplankton groups exposed to PAR. This event indicates for the first time an in situ biological source of CO in the ocean.

4752

Figure 14a to d present the vertical profiles of CO, isoprene, chlorophyll and phytoplankton species at four selected stations. The impact of the biomass observed on surface-seawater CO measurements has also been observed in the depth profiles, as illustrated in Fig. 14a and b at stations s124 and s167. At these stations (and five others not presented here), a deviation from the decreasing profile following the light penetration was found for CO. Among those stations, the maximum of chlorophyll *a* usually aligned with the deviation of CO concentration with depth (most pronounced at station 167), suggesting a biological origin of this secondary CO maximum. We note that sometimes the deviation of CO pattern occurred slightly above the maximum of chlorophyll *a*. For comparison, two other stations (s179 and s182), where no deviation was observed for CO, are reported in Fig. 14c and d.

Concerning vertical isoprene gradients, as shown in Fig. 9, the average profile of isoprene concentrations had a deep subsurface maximum that aligned with the maximum chlorophyll *a* concentration, reinforcing the conclusion that the secondary maximum observed for CO was due to biological production.

At station s124 measured on the Fram Strait close to Spitzbergen, a profile of isoprene showed two maxima, the first one at 5–10 m depth and the second one at 20–25 m depth, exactly as the chlorophyll *a* profile, which was represented by mostly *Phaeocystis*-type algae. Associated to the CO profiles of s167, a station also on the Fram Strait, the maximum isoprene value occurred at the maximum value of chlorophyll *a* concentration between 20 and 30 m depth. The peaks of isoprene seemed to be driven once again by *Phaeocystis*-type algae but also by dinoflagellates and to a lesser extent by diatom species and one species of chlorophyte. At station s179 (79.7° N, Fig. 14b), the isoprene depth profile indicated a maximum of concentration at 15 m depth, the same as the maximum of chlorophyll *a* concentration. This chlorophyll *a* maximum was driven by a combination of several algae groups, such as *Phaeocystis*, coccolithophorids, prasinophytes and dinoflagellates. Among those species, prasinophytes seemed to drive the isoprene concentration at 15 m depth. At station s182

4753

(Fig. 14c), the most northern station (79.9° N), the maxima of isoprene and chlorophyll *a* concentrations were governed by diatoms and coccolithophorids.

The maximum isoprene level was observed for most of the stations at the same depth as the chlorophyll *a* maximum, but sometimes it appeared slightly above this maximum. The offset between these maxima has already been observed previously by Bonsang et al. (1992) and Milne et al. (1995), who suggested that there might be no direct link between isoprene and chlorophyll and that isoprene could rather be produced by the degradation of an organic precursor. However, Moore et al. (1994) note that the total rate of photosynthesis is a function not only of chlorophyll content but also of the light intensity, which decreases exponentially through the water column. Therefore, these authors suggested observing the level of maximum isoprene lying above the chlorophyll maximum. Finally, McKay et al. (1996) and Shaw et al. (2003) assumed that isoprene appears during phytoplankton growth and is most likely produced either directly by the plankton or through the oxidation of exuded dissolved organic carbon.

From the vertical profiles of the compounds and their corresponding abundance in the water column, a biological production rate (Table 6) could be inferred according to the calculations described below. The estimations of the CO production through this secondary biological process are made by considering the difference  $\Delta Q$  in the water column content between the observed CO profile and the CO profile fitted without this secondary maximum (assuming a quasi-exponential decrease). This excess is then normalized to the chlorophyll concentration measured at these levels to obtain  $\mu\text{g}$  of CO per g of chlorophyll, and then, using the  $k$  factor estimated for the exchange term at the air-sea interface and the microbial consumption with a constant  $\mu$ , the production by biological processes  $P_{\text{CO,bio}}$  is given by a term derived from Eq. (3):

$$P_{\text{CO,bio}} = \Delta Q(k + \mu) \quad (7)$$

This calculation leads to values from 18 to 72  $\mu\text{mol CO g Chl } a^{-1} \text{ d}^{-1}$  (mean value  $41 \pm 20 \mu\text{mol CO g Chl } a^{-1} \text{ d}^{-1}$ ). Comparing the CO profiles to the

4754

species-concentration profiles, we have observed that *Phaeocystis*, dinoflagellates and to a lesser extent diatoms were dominant when this deviation appeared.

For isoprene, similar calculations were conducted in the mixed layer, and in this case, the only sink was the exchange with the atmosphere. Isoprene production rates are on the average of  $1.13 \mu\text{mol C}_5\text{H}_8 \text{ g Chl } a^{-1} \text{ d}^{-1}$  and of  $0.60 \mu\text{mol C}_5\text{H}_8 \text{ g Chl } a^{-1} \text{ d}^{-1}$  for the five stations where a secondary CO maximum was observed in the mixed layer. We can compare these production rates based on our in situ measurements with values from the literature based on laboratory experiments (Table 7).

The mean isoprene production rate was in the range of production by diatoms and coccolithophorids reported by Shaw et al. (2003) and Bonsang et al. (2010). However, we must note that the isoprene production was highly algae-group dependent, and only a few species were studied in the laboratory. Moreover, the light conditions of the laboratory experiments included PAR irradiance of approximately  $75 \text{ to } 100 \mu\text{E m}^{-2} \text{ s}^{-1}$ , which is slightly greater than the conditions of our field experiment.

Concerning CO, Gros et al. (2009) measured several species of diatoms, cyanobacteria, one species of coccolithophorid and one species of chlorophyte. The authors found production rates ranging from 19 to  $374 \mu\text{mol CO g Chl } a^{-1} \text{ d}^{-1}$  for diatom species (with a median value of  $33 \mu\text{mol CO g Chl } a^{-1} \text{ d}^{-1}$ ), between 115 and  $344 \mu\text{mol CO g Chl } a^{-1} \text{ d}^{-1}$  for cyanobacteria and values of 56 and  $6 \mu\text{mol CO g Chl } a^{-1} \text{ d}^{-1}$  for the coccolithophorid and chlorophyte, respectively. No *Phaeocystis* or dinoflagellates have been measured in the laboratory. The average value calculated from our five stations with an additional source of CO was in the lower range of the diatom production rates determined in the laboratory. Our observations were thus consistent with the occurrence of a secondary mechanism of CO production driven by in situ biological processes.

4755

## 6 Conclusions

A dataset of CO and NMHC concentrations combined with biological measurements in high latitudes of the Arctic Ocean is described. High variability of CO and propene was observed in the depth profiles and at the seawater surface. The photo-degradation of CDOM by light radiation was the main identified process for CO and alkene production, and the vertical profiles of CO and alkenes in the water column were consequently driven by light penetration. However, at the surface, the global solar radiation was not the main parameter that influenced the variability of the sea-surface concentrations; indeed, no CO or alkene diurnal cycles were observed. Polar water showed a significant enhancement of CO and alkene surface concentrations by a combination of two effects: a reduction of the mixed-layer depth, in accordance with a strong stratification and density gradient within the first 10 m, and an increase of the CDOM concentration.

Biomass activity was also found to be an important parameter. We have observed for the first time through in situ measurements that CO was directly produced by phytoplankton. Compared to laboratory studies, the biological production of CO was of the same order of magnitude as that previously estimated for diatoms. In addition to these observations, we have also confirmed the direct influence of biology on the production of isoprene and have shown that the isoprene production was species-dependent. However, further work is needed to better characterize the role of sea ice in the source of CO and NMHC and to identify the main sinks of isoprene and other NMHC in the water column.

## Appendix A

### Determination of the extraction yield

The theoretical extraction yield can be defined as the ratio of the mass of the NMHC extracted in the gas phase to the initial mass in the water analyzed. Assuming that the

4756





of Wanninkhof (1992):

$$K_w = 0.31 \cdot u^2 \left( \frac{Sc}{660} \right)^{-\frac{1}{2}} \quad (\text{B1})$$

where  $u$  ( $\text{m s}^{-1}$ ) is the wind velocity at 10 m. The Schmidt number  $Sc$  (dimensionless) is given by the ratio  $Sc = \frac{\nu}{D}$ , where  $\nu$  the kinematic viscosity of water (in  $\text{cm}^2 \text{s}^{-1}$ ) and  $D$  is the diffusivity of the considered species in water.  $D$ , which is dependent on temperature, is calculated by applying the classic Wilke and Chang (1955) equation:

$$D = 7.4 \times 10^{-8} \frac{\sqrt{\gamma M}}{\eta V_a^{0.6}} T \quad (\text{B2})$$

where

- $\eta$  is the viscosity of seawater (in centipoises or  $10^{-2} \text{ g cm}^{-1} \text{ s}^{-1}$ )
- $\gamma$  is the association factor (2.6 for water)
- $M$  is the molar mass of water in  $\text{g mol}^{-1}$
- $T$  is the temperature of seawater ( $^{\circ}\text{K}$ )
- $V_a$  is the molar volume of the considered species.

*Acknowledgements.* This project was funded by the Egide (Procopé) program common to the German and French Ministries of Foreign Affairs. We thank the captain and crew of the R/V *Polarstern* and the chief scientist Thomas Soltwedel for their support. We thank the AWI for supporting the experiment on board the R/V *Polarstern* and for access to logistic and data facilities. Special thanks are due to the Ferry box group from the Helmholtz Zentrum Geesthacht for the CDOM data and Gereon Budeus (AWI) for the density data. CNRS and CEA are acknowledged for additional support.

4759



The publication of this article is financed by CNRS-INSU.

## References

- Arnold, S. R., Spracklen, D. V., Williams, J., Yassaa, N., Sciare, J., Bonsang, B., Gros, V., Peeken, I., Lewis, A. C., Alvaïn, S., and Moulin, C.: Evaluation of the global oceanic isoprene source and its impacts on marine organic carbon aerosol, *Atmos. Chem. Phys.*, 9, 1253–1262, doi:10.5194/acp-9-1253-2009, 2009.
- Atkinson, R.: Tropospheric reactions of the haloalkyl radicals formed from hydroxyl radical reaction with a series of alternative fluorocarbons, in: Scientific Assessment of Stratospheric Ozone: 1989, World Meteorological Organization Global Ozone Research and Monitoring Project – Report No. 20, Volume II, 165–205, Appendix: AFEAS Report, Geneva, Switzerland, 1990.
- Ayers, G. P., Cainey, J. M., Gillett, R. W., Saltzman, E. S., and Hooper, M.: Sulfur dioxide and dimethyl sulfide in marine air at Cape Grim, Tasmania, *Tellus*, 49B, 292–299, 1997.
- Barlow, R. G., Cummings, D. G., and Gibb, S. W.: Improved resolution of mono- and divinyl chlorophylls a and b and zeaxanthin and lutein in phytoplankton extracts using reverse C-8 HPLC, *Mar. Ecol. Prog. Ser.*, 161, 303–307, 1997.
- Bates, T. S., Kelly, K. C., Johnson, J. E., and Gammon, R. H.: Regional and seasonal variations in the flux of oceanic carbon monoxide to the atmosphere, *J. Geophys. Res.*, 100, 23093–23101, doi:10.1029/95JD02737, 1995.
- Belzile, C., Johannessen, S. C., Gosselin, M., Demers, S., and Miller, W. L.: Ultraviolet attenuation by dissolved and particulate constituents of first-year ice during late spring in an arctic polynya, *Limnol. Oceanogr.*, 45, 1265–1273, doi:10.4319/lo.2000.45.6.1265, 2000.

4760

- Bidigare, R. R.: Analysis of algal chlorophylls and carotenoids, in: *Marine particles: Analysis and characterisation*, edited by: Hurd, D. C. and Spencer, D. W., American Geophysical Union, 119–123, 1991.
- Blindheim, J. and Rey, F.: Water-mass formation and distribution in the Nordic Seas during the 1990s, *ICES J. Mar. Sci.*, 61, 846–863, doi:10.1016/j.icesjms.2004.05.003, 2004.
- Bonsang, B., Kanakidou, M., Lambert, G., and Monfray, P.: The marine source of C<sub>2</sub>-C<sub>6</sub> aliphatic hydrocarbons, *J. Atmos. Chem.*, 6, 3–20, doi:10.1007/BF00048328, 1988.
- Bonsang, B., Polle, C., and Lambert, G.: Evidence of marine production of isoprene, *Geophys. Res. Lett.*, 19, 1129–1132, doi:10.1029/92GL00083, 1992.
- Bonsang, B., Polle, C., and Lambert, G.: Production of nonmethane hydrocarbons by seawater, *Ann. Inst. Oceanogr.*, 69, 125–128, 1993.
- Bonsang, B., Gros, V., Peeken, I., Yassaa, N., Bluhm, K., Zoellner, E., Sarda-Esteve, R., and Williams, J.: Isoprene emission from phytoplankton monocultures: the relationship with chlorophyll *a*, cell volume and carbon content, *Environ. Chem.*, 7, 554–563, doi:10.1071/EN09156, 2010.
- Broadgate, W. J., Liss, P. S., and Penkett, S. A.: Seasonal emissions of isoprene and other reactive hydrocarbon gases from the ocean, *Geophys. Res. Lett.*, 24, 2675–2678, doi:10.1029/97GL02736, 1997.
- Broadgate, W. J., Malin, G., Kupper, F. C., Thompson, A., and Liss, P. S.: Isoprene and other non-methane hydrocarbons from seaweeds: A source of reactive hydrocarbons to the atmosphere, *Mar. Chem.*, 88, 61–73, 2004.
- Carlsaw, N., Creasey, D. J., Heard, D. E., Lewis, A. C., McQuaid, J. B., Pilling, M. J., Monks, P. S., Bandy, B. J., and Penkett, S. A.: Modeling OH, HO<sub>2</sub>, and RO<sub>2</sub> radicals in the marine boundary layer – 1. Model construction and comparison with field measurements, *J. Geophys. Res.-Atmos.*, 104, 30241–30255, doi:10.1029/1999JD900783, 1999.
- Cauwet, G. and Sidorov, I.: The biogeochemistry of lena river: Organic carbon and nutrients distribution, *Mar. Chem.*, 53, 211–227, doi:10.1016/0304-4203(95)00090-9, 1996.
- Claeys, M., Graham, B., Vas, G., Wang, W., Vermeylen, R., Pashynska, V., Cafmeyer, J., Guyon, P., Andreae, M. O., Artaxo, P., and Maenhaut, W.: Formation of secondary organic aerosols through photooxidation of isoprene, *Science*, 303, 1173–1176, doi:10.1126/science.1092805, 2004.
- Conrad, R., Seiler, W., Bunse, G., and Giehl, H.: Carbon monoxide in sea-water (Atlantic Ocean), *J. Geophys. Res.-Oc. Atm.*, 87, 8839–8852, 1982.

4761

- Crutzen, P. J.: Global budgets for non-CO<sub>2</sub> greenhouse gases, *Environ. Monit. Assess.*, 31, 1–15, doi:10.1007/bf00547177, 1994.
- Day, D. A. and Faloona, I.: Carbon monoxide and chromophoric dissolved organic matter cycles in the shelf waters of the northern California upwelling system, *J. Geophys. Res.-Oceans*, 114, C01006, doi:10.1029/2007JC004590, 2009.
- Edney, E. O., Kleindienst, T. E., Jaoui, M., Lewandowski, M., Offenberg, J. H., Wang, W., and Claeys, M.: Formation of 2-methyl tetrols and 2-methylglyceric acid in secondary organic aerosol from laboratory irradiated isoprene/NO<sub>x</sub>/SO<sub>2</sub>/air mixtures and their detection in ambient PM (2.5) samples collected in the eastern united states, *Atmos. Environ.*, 39, 5281–5289, doi:10.1016/j.atmosenv.2005.05.031, 2005.
- Eilertsen, H.-C. and Holm-Hansen, O.: Effects of high latitude UV radiation on phytoplankton and nekton modelled from field measurements by simple algorithms, *Polar Res.*, 19, 173–182, doi:10.1111/j.1751-8369.2000.tb00341.x, 2000.
- Erickson, D. J. and Taylor, J. A.: 3-D tropospheric CO modeling – the possible influence of the ocean, *Geophys. Res. Lett.*, 19, 1955–1958, doi:10.1029/92gl01475, 1992.
- Fichot, C. G. and Miller, W. L.: An approach to quantify depth-resolved marine photochemical fluxes using remote sensing: Application to carbon monoxide (CO) photoproduction, *Remote Sens. Environ.*, 114, 1363–1377, doi:10.1016/j.rse.2010.01.019, 2010.
- Frey, K. E. and Smith, L. C.: Amplified carbon release from vast west siberian peatlands by 2100, *Geophys. Res. Lett.*, 32, L09401, doi:10.1029/2004gl022025, 2005.
- Gantt, B., Meskhidze, N., and Kamykowski, D.: A new physically-based quantification of marine isoprene and primary organic aerosol emissions, *Atmos. Chem. Phys.*, 9, 4915–4927, doi:10.5194/acp-9-4915-2009, 2009.
- Gantt, B., Meskhidze, N., Zhang, Y., and Xu, J.: The effect of marine isoprene emissions on secondary organic aerosol and ozone formation in the coastal United States, *Atmos. Environ.*, 44, 115–121, doi:10.1016/j.atmosenv.2009.08.027, 2010.
- Gibson, J. A. E., Vincent, W. F., and Pienitz, R.: Hydrologic control and diurnal photobleaching of CDOM in a subarctic lake, *Arch. Hydrobiol.*, 152, 143–159, 2001.
- Gros, V., Peeken, I., Bluhm, K., Zollner, E., Sarda-Esteve, R., and Bonsang, B.: Carbon monoxide emissions by phytoplankton: Evidence from laboratory experiments, *Environ. Chem.*, 6, 369–379, doi:10.1071/en09020, 2009.
- Guenther, A., Hewitt, C. N., Erickson, D., Fall, R., Geron, C., Gradel, T., Harley, P., Klinger, L., Lerdau, M., McKay, W. A., Pierce, T., Scholes, B., Steinbrecher, R., Tallamraju, R., Taylor,

4762

- J., and Zimmerman, P.: A global model of natural volatile organic-compound emissions, *J. Geophys. Res.-Atmos.*, 100, 8873–8892, doi:10.1029/94JD02950, 1995.
- Guenther, A., Karl, T., Harley, P., Wiedinmyer, C., Palmer, P. I., and Geron, C.: Estimates of global terrestrial isoprene emissions using MEGAN (Model of Emissions of Gases and Aerosols from Nature), *Atmos. Chem. Phys.*, 6, 3181–3210, doi:10.5194/acp-6-3181-2006, 2006.
- Häder, D.-P., Kumar, H. D., Smith, R. C., and Worrest, R. C.: Effects of solar UV radiation on aquatic ecosystems and interactions with climate change, *Photochem. Photobiol. Sci.*, 6, 267–285, 2007.
- Hudson, E. D. and Ariya, P. A.: Measurements of non-methane hydrocarbons, DOC in surface ocean waters and aerosols over the Nordic seas during Polarstern cruise ARK-XX/1 (2004), *Chemosphere*, 69, 1474–1484, doi:10.1016/j.chemosphere.2007.04.056, 2007.
- Jeffrey, S. W. and Vesk, M.: Introduction to marine phytoplankton and their pigment signatures, in: *Phytoplankton pigments in oceanography: Guideline to modern methods.*, edited by: Jeffrey, S. W., Mantoura, R. F. C., and Wright, S. W., 10, UNESCO Publishing, Paris, 37–84, 1997.
- Johnson, J. E. and Bates, T. S.: Sources and sinks of carbon monoxide in the mixed layer of the tropical South Pacific Ocean, *Global Biogeochem. Cy.*, 10, 347–359, doi:10.1029/96GB00366, 1996.
- Jones, R. D.: Carbon-monoxide and methane distribution and consumption in the photic zone of the Sargasso Sea, *Deep-Sea Res. Part a-Oceanographic Research Papers*, 38, 625–635, doi:10.1016/0198-0149(91)90002-w, 1991.
- Kanakidou, M., Seinfeld, J. H., Pandis, S. N., Barnes, I., Dentener, F. J., Facchini, M. C., Van Dingenen, R., Ervens, B., Nenes, A., Nielsen, C. J., Swietlicki, E., Putaud, J. P., Balkanski, Y., Fuzzi, S., Horth, J., Moortgat, G. K., Winterhalter, R., Myhre, C. E. L., Tsigaridis, K., Vignati, E., Stephanou, E. G., and Wilson, J.: Organic aerosol and global climate modelling: a review, *Atmos. Chem. Phys.*, 5, 1053–1123, doi:10.5194/acp-5-1053-2005, 2005.
- Kettle, A. J.: Diurnal cycling of carbon monoxide (CO) in the upper ocean near Bermuda, *Ocean Model.*, 8, 337–367, doi:10.1016/j.ocemod.2004.01.003, 2005.
- Kroll, J. H. and Seinfeld, J. H.: Chemistry of secondary organic aerosol: Formation and evolution of low-volatility organics in the atmosphere, *Atmos. Environ.*, 42, 3593–3624, doi:10.1016/j.atmosenv.2008.01.003, 2008.

4763

- Lee, R. F. and Baker, J.: Ethylene and ethane production in an estuarine river – formation from the decomposition of polyunsaturated fatty-acids, *Mar. Chem.*, 38, 25–36, doi:10.1016/0304-4203(92)90065-i, 1992.
- Lewis, A. C., McQuaid, J. B., Carslaw, N., and Pilling, M. J.: Diurnal cycles of short-lived tropospheric alkenes at a north Atlantic coastal site, *Atmos. Environ.*, 33, 2417–2422, doi:10.1016/S1352-2310(98)00429-4, 1999.
- Lewis, A. C., Carpenter, L. J., and Pilling, M. J.: Nonmethane hydrocarbons in Southern Ocean boundary layer air, *J. Geophys. Res.-Atmos.*, 106, 4987–4994, doi:10.1029/2000JD900634, 2001.
- Liakakou, E., Vrekoussis, M., Bonsang, B., Donousis, C., Kanakidou, M., and Mihalopoulos, N.: Isoprene above the Eastern Mediterranean: Seasonal variation and contribution to the oxidation capacity of the atmosphere, *Atmos. Environ.*, 41, 1002–1010, doi:10.1016/j.atmosenv.2006.09.034, 2007.
- Linnenbom, V. J., Swinnerton, J. W., and Lamontagne, R. A.: Ocean as a source for atmospheric carbon-monoxide, *J. Geophys. Res.*, 78, 5333–5340, doi:10.1029/JC078i024p05333, 1973.
- Logan, J., Prather, M. J., Wofsy, S. C., and McElroy, M. B.: Tropospheric chemistry: A global perspective, *J. Geophys. Res.-Atmos.*, 86, 7210–7254, doi:10.1029/JC086iC08p07210, 1981.
- Mackey, M. D., Mackey, D. J., Higgings, H. W., and Wright, S. W.: “CHEMTAX”- a program for estimating class abundances from chemical markers: Application to HPLC measurements of phytoplankton, *Mar. Ecol.-Prog. Ser.*, 144, 265–283, doi:10.3354/meps144265, 1996.
- McKay, W. A., Turner, M. F., Jones, B. M. R., and Halliwell, C. M.: Emissions of hydrocarbons from marine phytoplankton – some results from controlled laboratory experiments, *Atmos. Environ.*, 30, 2583–2593, doi:10.1016/1352-2310(95)00433-5, 1996.
- Milne, P. J., Riemer, D. D., Zika, R. G., and Brand, L. E.: Measurement of vertical-distribution of isoprene in surface seawater, its chemical fate, and its emission from several phytoplankton monocultures, *Mar. Chem.*, 48, 237–244, doi:10.1016/0304-4203(94)00059-m, 1995.
- Moore, R. M. and Zafiriou, O. C.: Photochemical production of methyl iodide in seawater, *J. Geophys. Res.-Atmos.*, 99, 16415–16420, doi:10.1029/94JD00786, 1994.
- Müller, J.-F., Stavrakou, T., Wallens, S., De Smedt, I., Van Roozendaal, M., Potosnak, M. J., Rinne, J., Munger, B., Goldstein, A., and Guenther, A. B.: Global isoprene emissions estimated using MEGAN, ECMWF analyses and a detailed canopy environment model, *Atmos. Chem. Phys.*, 8, 1329–1341, doi:10.5194/acp-8-1329-2008, 2008.

4764

- Nürnberg, D., Wollenburg, I., Dethleff, D., Eicken, H., Kassens, H., Letzig, T., Reimnitz, E., and Thiede, J.: Sediments in Arctic sea ice: Implications for entrainment, transport and release, *Mar. Geol.*, 119, 185–214, doi:10.1016/0025-3227(94)90181-3, 1994.
- Ohta, K.: Diurnal variations of carbon monoxide in the Equatorial Pacific upwelling region, *J. Oceanogr.*, 53, 173–178, 1997.
- Opsahl, S., Benner, R., and Amon, R. M. W.: Major flux of terrigenous dissolved organic matter through the Arctic Ocean, *Limnol. Oceanogr.*, 44, 2017–2023, doi:10.4319/lo.1999.44.8.2017, 1999.
- Palmer, P. I. and Shaw, S. L.: Quantifying global marine isoprene fluxes using modis chlorophyll observations, *Geophys. Res. Lett.*, 32, L09805, doi:10.1029/2005GL022592, 2005.
- Plass-Dulmer, C., Koppmann, R., Ratte, M., and Rudolph, J.: Light nonmethane hydrocarbons in seawater, *Global Biogeochem. Cy.*, 9, 79–100, doi:10.1029/94GB02416, 1995.
- Prather, M. J.: Time scales in atmospheric chemistry: Theory, GWPs for CH<sub>4</sub> and CO, and runaway growth, *Geophys. Res. Lett.*, 23, 2597–2600, doi:10.1029/96gl02371, 1996.
- Prather, M. J., Ehhalt, D., Dentener, F., Derwent, R., Dlugokencky, E., Holland, E., Isaksen, I., Katima, J., Kirchhoff, V., Matson, P., Midgley, P., Wang, M.: Chapter 4: Atmospheric chemistry and greenhouse gases, in: *Climate Change 2001: The scientific basis*, edited by: Houghton, J.T., Ding, Y., Griggs, D. J., Noguer, M., van der Linden, P. J., Dai, X., Maskell, K., and Johnson, C. A., Contribution of working group 1 to the third assessment report of the inter-governmental panel on climate change, Cambridge University Press, Cambridge, 239–287, 2001.
- Rasmussen, R. A. and Went, F. W.: Volatile organic material of plant origin in atmosphere, *P. Natl. Acad. Sci. USA*, 53, 215–220, doi:10.1073/pnas.53.1.215, 1965.
- Ratte, M., Plass-Dülmer, C., Koppmann, R., Rudolph, J., and Denga, J.: Production mechanism of C<sub>2</sub>-C<sub>4</sub> hydrocarbons in seawater – field-measurements and experiments, *Global Biogeochem. Cy.*, 7, 369–378, doi:10.1029/93gb00054, 1993.
- Ratte, M., Bujok, O., Spitz, A., and Rudolph, J.: Photochemical alkene formation in seawater from dissolved organic carbon: Results from laboratory experiments, *J. Geophys. Res.-Atmos.*, 103, 5707–5717, doi:10.1029/97JD03473, 1998.
- Retamal, L., Vincent, W. F., Martineau, C., and Osburn, C. L.: Comparison of the optical properties of dissolved organic matter in two river-influenced coastal regions of the Canadian Arctic, *Estuar. Coast. Shelf Sci.*, 72, 261–272, doi:10.1016/j.ecss.2006.10.022, 2007.
- Rhee, T. S.: The process of air-water exchange and its application, Ph.D. Thesis, 2000.

4765

- Riemer, D. D., Milne, P. J., Zika, R. G., and Pos, W. H.: Photoproduction of nonmethane hydrocarbons (NMHCs) in seawater, *Mar. Chem.*, 71, 177–198, doi:10.1016/S0304-4203(00)00048-7, 2000.
- Rudels, B., Jones, E. P., Schauer, U., and Eriksson, P.: Atlantic sources of the Arctic Ocean surface and halocline waters, *Polar Res.*, 23, 181–208, doi:10.1111/j.1751-8369.2004.tb00007.x, 2004.
- Rudolph, J. and Ehhalt, D. H.: Measurements of C<sub>2</sub>-C<sub>5</sub> hydrocarbons over the North Atlantic, *J. Geophys. Res.-Oc. Atm.*, 86, 1959–1964, doi:10.1029/JC086iC12p11959, 1981.
- Sander, R.: *Compilation of Henry's Law Constants for Inorganic and Organic Species of Potential Importance in Environmental Chemistry*, 20, Max-Planck Institute of Chemistry, Air Chemistry Dept., available at: <http://www.rolf-sander.net/henry/henry.pdf> (last access: 6 September 2011), 1999.
- Schlichtholz, P. and Houssais, M. N.: An inverse modeling study in fram strait. Part II: Water mass distribution and transports, *Deep-Sea Res. Part II-Topical Studies in Oceanography*, 46, 1137–1168, doi:10.1016/s0967-0645(99)00017-x, 1999.
- Schobert, B. and Elstner, E. F.: Production of hexanal and ethane by phaeodactylum-triconutum and its correlation to fatty-acid oxidation and bleaching of photosynthetic pigments, *Plant Physiol.*, 66, 215–219, doi:10.1104/pp.66.2.215, 1980.
- Scully, N. M. and Miller, W. L.: Spatial and temporal dynamics of colored dissolved organic matter in the north water polynya, *Geophys. Res. Lett.*, 27, 1009–1011, doi:10.1029/1999gl007002, 2000.
- Shaw, S. L., Chisholm, S. W., and Prinn, R. G.: Isoprene production by prochlorococcus, a marine cyanobacterium, and other phytoplankton, *Mar. Chem.*, 80, 227–245, doi:10.1016/s0304-4203(02)00101-9, 2003.
- Gantt, B. and Meskhidze, N.: Production and emissions of marine isoprene and monoterpenes: A review, *Adv. Meteor.*, 1–24, 408696, doi:10.1155/2010/408696, 2010.
- Stramski, D., Reynolds, R. A., Babin, M., Kaczmarek, S., Lewis, M. R., Röttgers, R., Sciandra, A., Stramska, M., Twardowski, M. S., Franz, B. A., and Claustre, H.: Relationships between the surface concentration of particulate organic carbon and optical properties in the eastern South Pacific and eastern Atlantic Oceans, *Biogeosciences*, 5, 171–201, doi:10.5194/bg-5-171-2008, 2008.

4766

- Stubbins, A., Uhera, G., Kitidis, V., Law, C. S., Upstill-Goddard, R. C., and Woodward, E. M. S.: The open-ocean source of atmospheric carbon monoxide, *Deep-Sea Res. Part II-Topical Studies in Oceanography*, 53, 1685–1694, doi:10.1016/j.dsr2.2006.05.010, 2006.
- 5 Swinnerton, J. W. and Lamontagne, R. A.: Carbon monoxide in south pacific ocean, *Tellus*, 26, 136–142, doi:10.3402/tellusa.v26i1-2.9744, 1974.
- Swinnerton, J. W., Linnenbom, V. J., and Lamontagne, R. A.: Distribution of carbon monoxide between atmosphere and ocean, *Anna. NY Acad. Sci.*, 174, 96–101, doi:10.1111/j.1749-6632.1970.tb49776.x, 1970.
- Thompson, A. M.: The oxidizing capacity of the earths atmosphere - probable past and future changes, *Science*, 256, 1157–1165, doi:10.1126/science.256.5060.1157, 1992.
- 10 Tsigaridis, K. and Kanakidou, M.: Global modelling of secondary organic aerosol in the troposphere: a sensitivity analysis, *Atmos. Chem. Phys.*, 3, 1849–1869, doi:10.5194/acp-3-1849-2003, 2003.
- Wängberg, S.-A., Andreasson, K. I. M., Gustavson, K., Reinthaler, T., and Henriksen, P.: UV-B effects on microplankton communities in Kongfjord, Svalbard – A mesocosm experiment, *J. Exp. Mar. Biol. Ecol.*, 365, 156–163, doi:10.1016/j.jembe.2008.08.010, 2008.
- Wanninkhof, R.: Relationship between wind-speed and gas-exchange over the ocean, *J. Geophys. Res.-Oceans*, 97, 7373–7382, doi:10.1029/92JC00188, 1992.
- Wheeler, P. A., Watkins, J. M., and Hansing, R. L.: Nutrients, organic carbon and organic nitrogen in the upper water column of the arctic ocean: Implications for the sources of dissolved organic carbon, *Deep-Sea Res. Part II-Topical Studies in Oceanography*, 44, 1571–1592, doi:10.1016/s0967-0645(97)00051-9, 1997.
- 20 Wilke, C. R. and Chang, P.: Correlation of diffusion coefficients in dilute solutions, *AIChE Journal*, 1, 264–270, doi:10.1002/AIC.690010222, 1955.
- Wilson, D. F., Swinnerton, J., and Lamontagne, R.: Production of carbon monoxide and gaseous hydrocarbons in seawater - relation to dissolved organic carbon, *Science*, 168, 1576–1577, doi:10.1126/science.168.3939.1577, 1970.
- Xie, H. X., Zafiriou, O. C., Wang, W., and Taylor, C. D.: A simple automated continuous flow equilibration method for measuring carbon monoxide in seawater, *Environ. Sci. Technol.*, 35, 1475–1480, doi:10.1021/es001656v, 2001.
- 30 Xie, H. X., Belanger, S., Demers, S., Vincent, W. F., and Papakyriakou, T. N.: Photobiogeochemical cycling of carbon monoxide in the southeastern beaufort sea in spring and autumn, *Limnol. Oceanogr.*, 54, 234–249, doi:10.4319/lo.2009.54.1.0234, 2009.

4767

- Yang, G.-P., Ren, C.-Y., Lu, X.-L., Liu, C.-Y., and Ding, H.-B.: Distribution, flux, and photoproduction of carbon monoxide in the East China Sea and Yellow Sea in spring, *J. Geophys. Res.*, 116, C02001, doi:10.1029/2010JC006300, 2011.
- Yaws, C. L. and Yang, H.-C.: Henry's law constant for compound in water. In C. L. Yaws, editor, 5 *Thermodynamic and Physical Property Data*, pages 181–206. Gulf Publishing Company, Houston, TX, 1992.
- Yaws, C. L., Yang, H. C., and Xiang, P.: Henry's law constants for organic 362 compounds in water, *Chem. Eng.*, 98, 179–185, 1991.
- Zafiriou, O. C., Andrews, S. S., and Wang, W.: Concordant estimates of oceanic carbon monoxide source and sink processes in the pacific yield a balanced global "Blue-water" CO budget, *J. Global Biogeochem. Cy.*, 17, 1015, doi:10.1029/2001gb001638, 2003.
- 10 Zafiriou, O. C., Xie, H., Nelson, N. B., Najjar, R. G., and Wang, W.: Diel carbon monoxide cycling in the upper Sargasso Sea near Bermuda at the onset of spring and in midsummer, *Limnol. Oceanogr.*, 53, 835–850, doi:10.4319/lo.2008.53.2.0835, 2008.
- 15 Zimmerman, P. R., Greenberg, J. P., and Westberg, C. E.: Measurements of atmospheric hydrocarbons and biogenic emission fluxes in the Amazon boundary-layer, *J. Geophys. Res.-Atmos.*, 93, 1407–1416, doi:10.1029/JD093iD02p01407, 1988.
- Zuo, Y. and Jones, R. D.: Formation of carbon-monoxide by photolysis of dissolved marine organic material and its significance in the carbon cycling of the oceans, *Naturwissenschaften*, 20 82, 472–474, doi:10.1007/BF01131598, 1995.

4768

**Table 1.** Classification of water masses (adapted from Schlichtholz and Houssais, 1999).

Water mass	Temperature	Salinity
Atlantic water with low salinity (AWs)	$\Theta > 5\text{ }^{\circ}\text{C}$	$S < 34.4$
Warm Atlantic Water (WAW)	$\Theta > 2\text{ }^{\circ}\text{C}$	$S > 34.91$
Fresh Atlantic Water (FAW)	$\Theta > 1\text{ }^{\circ}\text{C}$	$34.4 < S < 34.91$
Polar Water (PW)	$\Theta < 0\text{ }^{\circ}\text{C}$	$S < 34.7$
	$\Theta > 0\text{ }^{\circ}\text{C}$	$S < 34.4$

4769

**Table 2.** Theoretical and experimental extraction yields for carbon monoxide and NMHC in our experimental conditions. Henry's law constants were taken from Sander (1999, available at: <http://www.rolf-sander.net/henry/henry.pdf>).

Compound	Henry's constant at 25 °C $\text{mol l}^{-1} \text{atm}^{-1}$	Theoretical extraction yield (%)	Experimental extraction yield (%)	Detection limit [NMHC] <sub>min</sub>
CO	$9.5 \times 10^{-4}$	97.7	56	0.08 $\text{nmol l}^{-1}$
Ethene	$4.7 \times 10^{-3}$	90.0	90	0.93 $\text{pmol l}^{-1}$
Propene	$4.8 \times 10^{-3}$	89.6	88	0.61 $\text{pmol l}^{-1}$
1-butene	$4.7 \times 10^{-3}$	91.2	75	0.79 $\text{pmol l}^{-1}$
Isobutene	$4.7 \times 10^{-3}$	89.8	74	1.16 $\text{pmol l}^{-1}$
1-pentene	$2.5 \times 10^{-3}$	94.3	78	2.11 $\text{pmol l}^{-1}$
Isoprene	$1.3 \times 10^{-2}$	76.1	64	5.14 $\text{pmol l}^{-1}$
Propane	$1.5 \times 10^{-3}$	95.6	95	1.47 $\text{pmol l}^{-1}$
n-butane	$1.2 \times 10^{-3}$	97.2	95	1.13 $\text{pmol l}^{-1}$
n-pentane	$8.0 \times 10^{-4}$	98.1	96	1.45 $\text{pmol l}^{-1}$

4770

**Table 3.** Mean and maximum concentrations of CO and NMHC recorded during the cruise.

	(nmol l <sup>-1</sup> )	Mean ± 1 SD	Maximal value
	CO	4.2 ± 3	17.5
Alkenes	(pmol l <sup>-1</sup> )	Mean ± 1 SD	Maximal value
	Propene	80 ± 58	322
	1-butene	10 ± 13	101
	Isobutene	24 ± 20	210
	1-pentene	8 ± 12	130
	Isoprene	26 ± 31	541
Alkenes	Propane	11 ± 32	451
	Isobutane	3 ± 20	320
	n-butane	24 ± 96	1013
	n-pentane	12 ± 11	64

4771

**Table 4.** CO and NMHC mean concentrations (± 1 standard deviation) sorted by water masses.

	Atlantic Water, low salinity	Polar Water	Fresh Atlantic Water	Warm Atlantic Water
CO (nmol l <sup>-1</sup> )	2.5 ± 1.7	6.5 ± 3.2	3.4 ± 2.4	3.3 ± 2.2
propene (pmol l <sup>-1</sup> )	63.6 ± 23.8	124.8 ± 60.6	58.4 ± 36.1	51.2 ± 49.8
1-butene (pmol l <sup>-1</sup> )	5.8 ± 3.2	21.1 ± 15.6	4.8 ± 6.4	3.7 ± 5.2
isobutene (pmol l <sup>-1</sup> )	12.8 ± 9.8	27.8 ± 17.9	20.4 ± 12.5	26.8 ± 28.1
1-pentene (pmol l <sup>-1</sup> )	3.3 ± 2.6	13.4 ± 10.1	6.4 ± 15.0	3.4 ± 11.2
isoprene (pmol l <sup>-1</sup> )	23.4 ± 31.0	14.5 ± 11.5	24.8 ± 19.1	42.5 ± 49.6

4772

**Table 5.** Quantum yields and budget of CO and alkenes in the mixed layer. The quantum yield values are (1) from Zafiriou et al. (2003) and (2) from Riemer et al. (2000).  $k$  is calculated for an average surface temperature of 3.5 °C, an average wind speed of 9 m s<sup>-1</sup> and a mixed layer of 20 m. See the text and Eq. (3) for details.

Species	Quantum yield $\Phi$	$C_{ML}$ (mol l <sup>-1</sup> )	$k$ (s <sup>-1</sup> ) at 3.5 °C	$\mu$ (s <sup>-1</sup> )	$R = C_{ML}(k + \mu)/\Phi$
CO	$1.80 \times 10^{-5}$ (1)	$4.2 \times 10^{-9}$	$2.3 \times 10^{-6}$	$5.7 \times 10^{-6}$	$1.87 \times 10^{-9}$
Propene	$1.13 \times 10^{-7}$ (2)	$80 \times 10^{-12}$	$1.9 \times 10^{-6}$	0	$1.35 \times 10^{-9}$
isobutene	$0.23 \times 10^{-7}$ (2)	$24 \times 10^{-12}$	$1.7 \times 10^{-6}$	0	$1.77 \times 10^{-9}$
1-butene	$0.09 \times 10^{-7}$ (2)	$10 \times 10^{-12}$	$1.7 \times 10^{-6}$	0	$1.89 \times 10^{-9}$

4773

**Table 6.** CO production rate ( $\mu\text{g CO g Chl a}^{-1} \text{h}^{-1}$  and  $\mu\text{mol CO g Chl a}^{-1} \text{d}^{-1}$ ) calculated for the five stations at which a biological production of CO was observed in the mixed layer.  $Z_{ML}$  is the depth of the mixed layer. For isoprene, the average and median production rate in the mixed layer was also calculated for all of the depth profiles.

Station	$Z_{ML}$ (m)	Ratio CO/Chl (g CO g Chl a <sup>-1</sup> )	CO Production $\mu\text{g CO g Chl a}^{-1} \text{h}^{-1}$	CO Production $\mu\text{mol CO g Chl a}^{-1} \text{d}^{-1}$	Isoprene Production $\mu\text{mol C}_5\text{H}_8 \text{ g Chl a}^{-1} \text{d}^{-1}$
s124	30	1,85E-03	40	34	0.41
s139	45	2,08E-03	45	39	0.83
s167	50	9,60E-04	22	18	0.98
s170	40	4,00E-03	84	72	-
s229	30	2,46E-03	52	44	0.19
Average (these 5 stations)			49	41	0.60
Average (median) for all of the depth profiles					1.13 (0.41)

4774





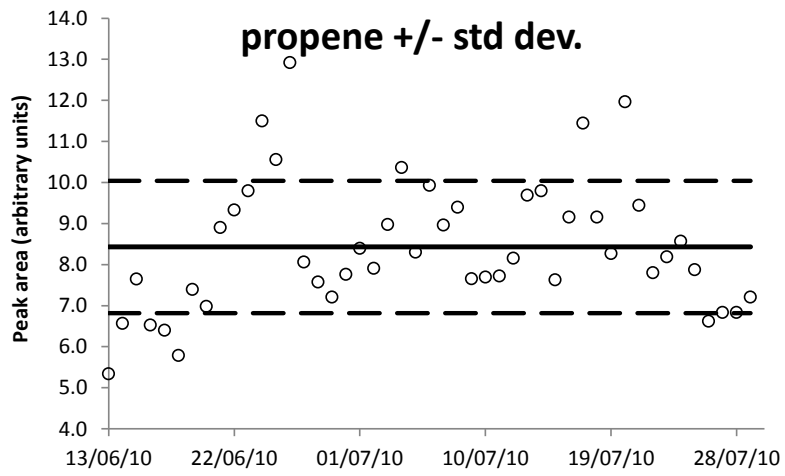


**Fig. 2.** Response of the detector to multiple injections of propene from the NPL calibration gas.

4777

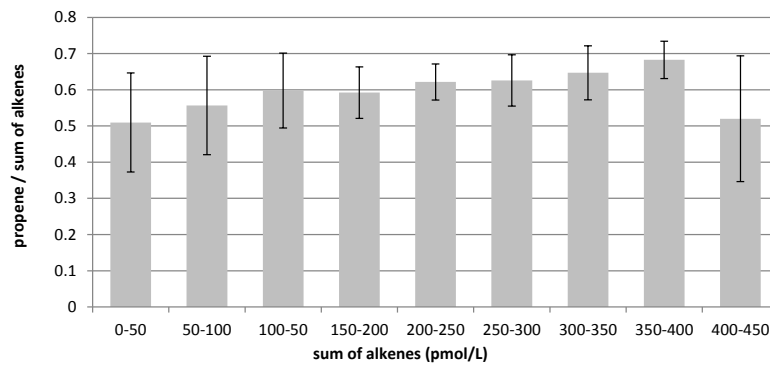


**Fig. 3.** Propene versus total light alkenes plotted against the total concentration of alkenes.

4778

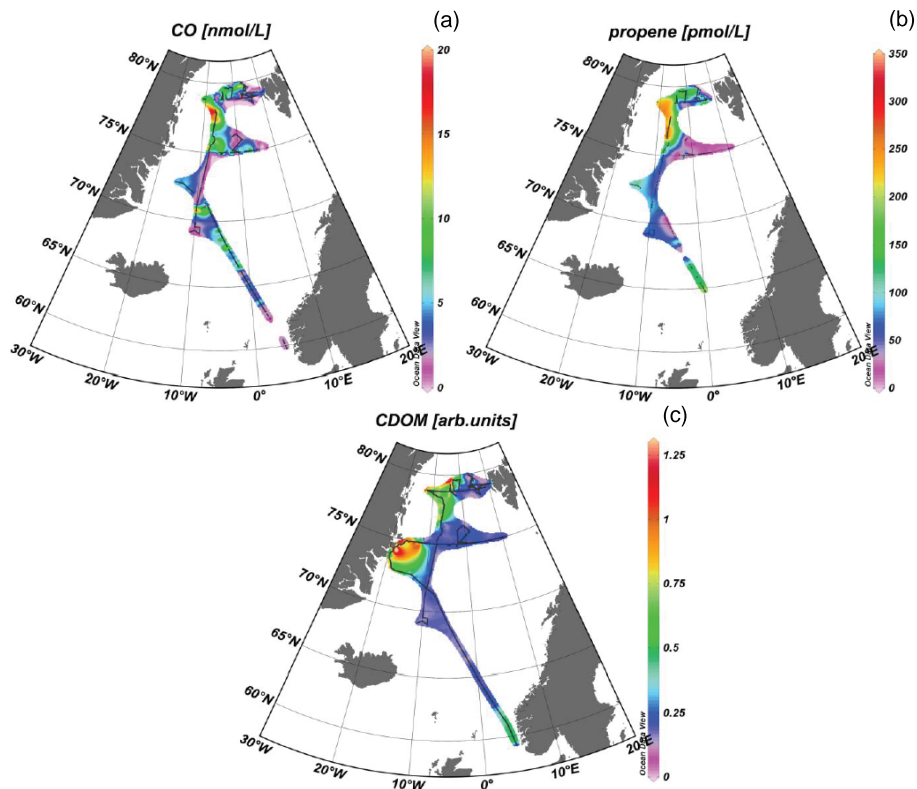


**Fig. 4.** Distributions of CO (a), propene (b) and CDOM (c) concentrations in surface waters (at a depth of 6 m) throughout the study area.

4779

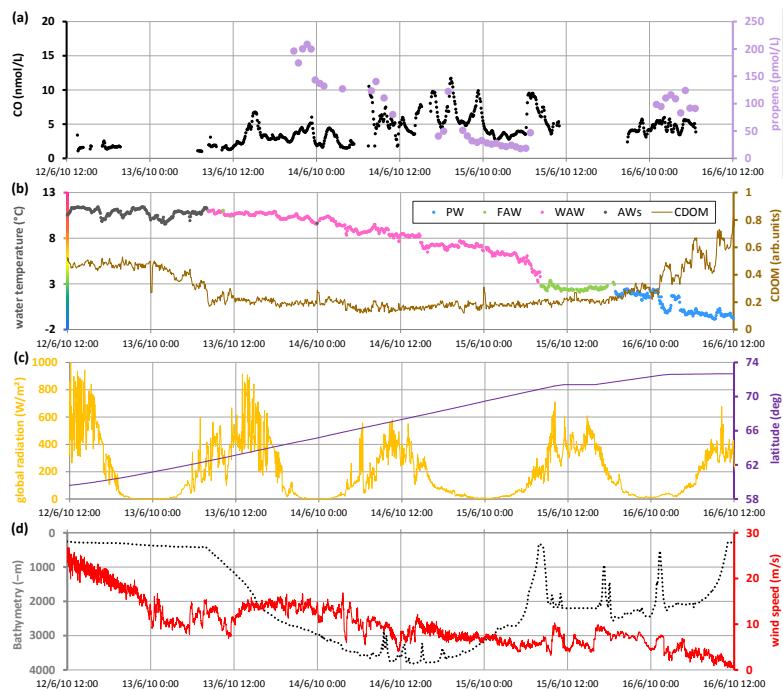


**Fig. 5.** Section 1. (a) Sea-surface CO ( $\text{nmol l}^{-1}$ ) and propene ( $\text{pmol l}^{-1}$ ) concentrations; (b) sea-surface temperature ( $^{\circ}\text{C}$ ), a classification of water masses (PW = Polar water, FAW = Fresh Atlantic Water, WAW = Warm Atlantic Water and AWs = Atlantic Water with low salinity) and CDOM levels (in arbitrary units); (c) total radiation ( $\text{W m}^{-2}$ ) and latitude (deg); and (d) bathymetry (m) and wind speed ( $\text{m s}^{-1}$ ).

4780

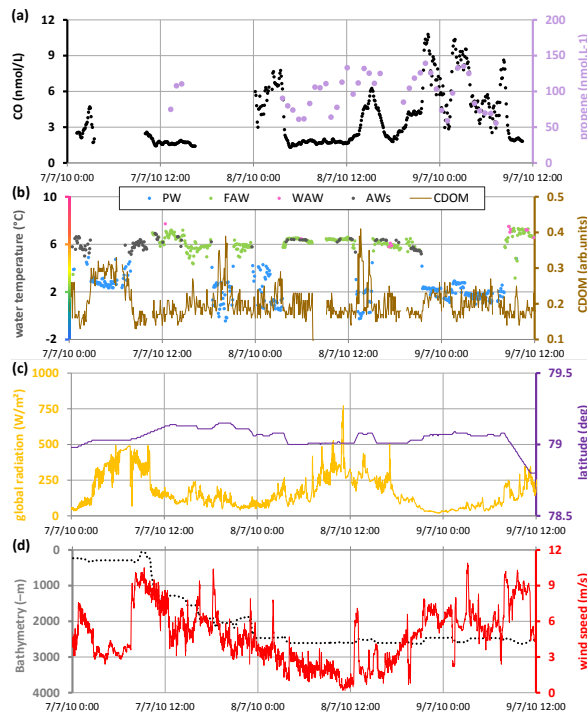


**Fig. 6.** Section 3. (a) Sea-surface CO ( $\text{nmol l}^{-1}$ ) and propene ( $\text{pmol L}^{-1}$ ) concentrations; (b) sea-surface temperature ( $^{\circ}\text{C}$ ), a classification of water masses (PW = Polar water, FAW = Fresh Atlantic Water, WAW = Warm Atlantic Water and AWs = Atlantic Water with low salinity) and CDOM levels (in arbitrary units); (c) total radiation ( $\text{W m}^{-2}$ ) and latitude (deg); and (d) bathymetry (m) and wind speed ( $\text{m s}^{-1}$ ).

4781

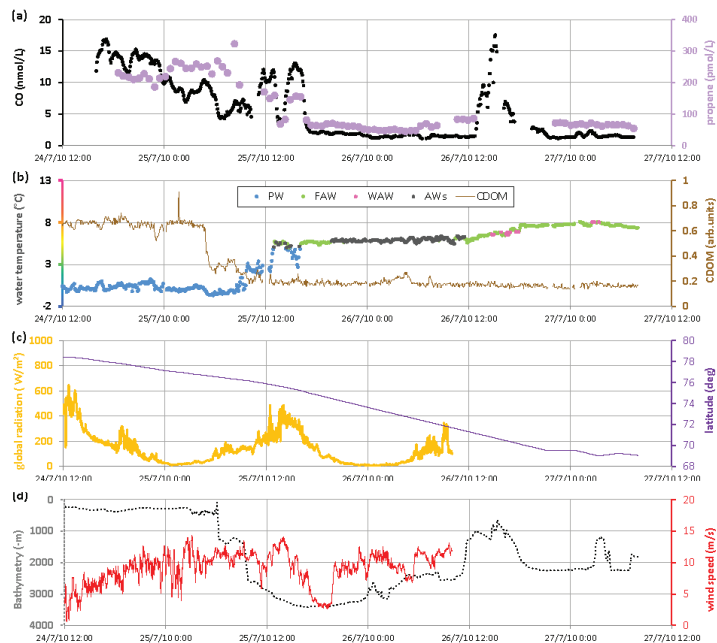


**Fig. 7.** Section 4. (a) Sea-surface CO ( $\text{nmol l}^{-1}$ ) and propene ( $\text{pmol l}^{-1}$ ) concentrations, (b) sea-surface temperature ( $^{\circ}\text{C}$ ), a classification of water masses (PW = Polar water, FAW = Fresh Atlantic Water, WAW = Warm Atlantic Water and AWs = Atlantic Water with low salinity) and CDOM levels (in arbitrary units); (c) total radiation ( $\text{W m}^{-2}$ ) and latitude (deg); and (d) bathymetry (m) and wind speed ( $\text{m s}^{-1}$ ).

4782

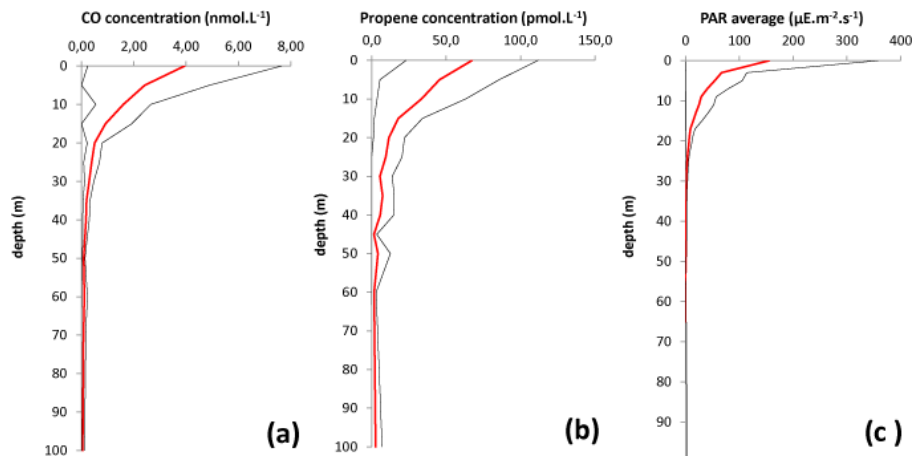


**Fig. 8.** Mean vertical profiles (in red)  $\pm$  standard deviation (in black) of CO **(a)** and propene **(b)** concentrations and the vertical distribution of PAR **(c)** for the whole cruise.

4783

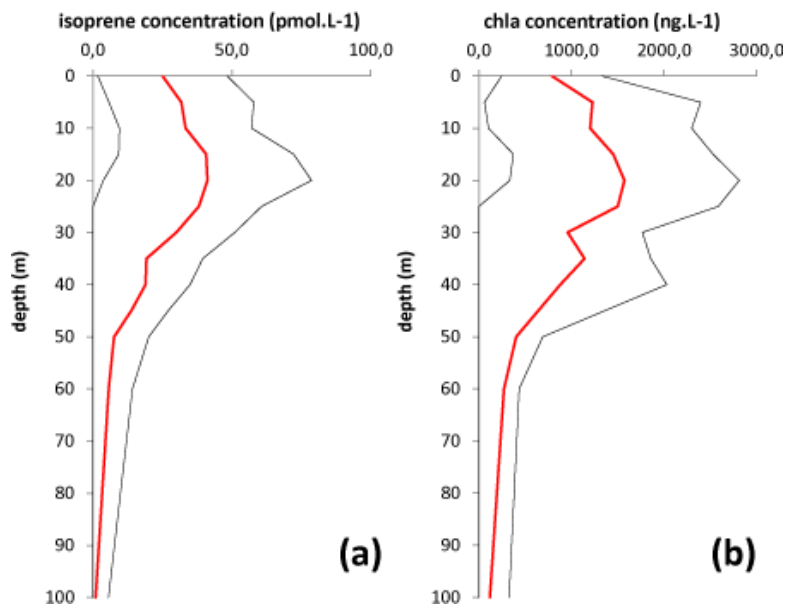


**Fig. 9.** Vertical profiles of mean isoprene **(a)** and chlorophyll *a* **(b)** concentrations for the whole cruise. Red lines represent mean concentrations, and dark lines correspond to the standard deviation.

4784

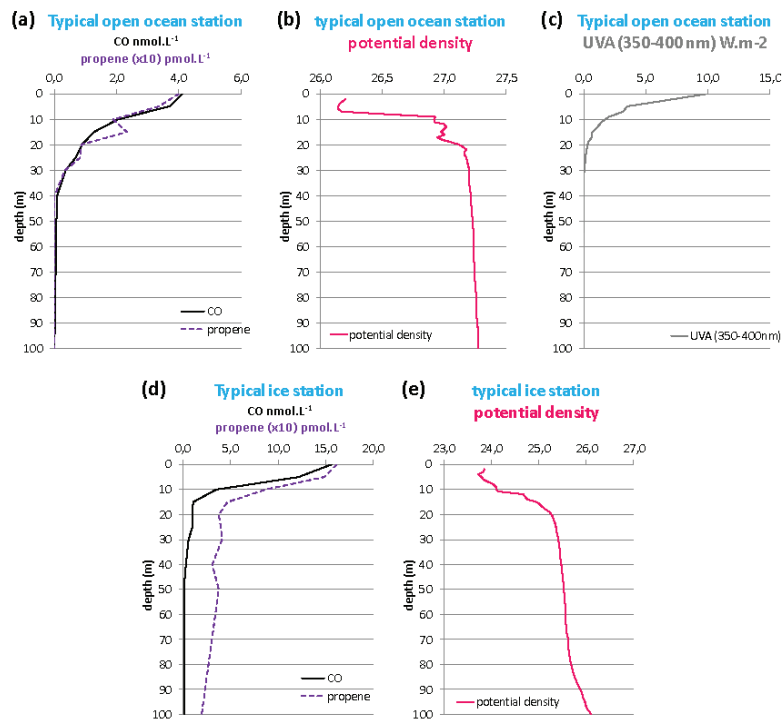


**Fig. 10.** CO (nmol L<sup>-1</sup>) and propene (pmol L<sup>-1</sup>) (a, d) concentrations and potential densities (b, e) of a typical open-ocean station (s194) and a typical ice station (s237). Vertical profile of UVA (from 350 to 400 nm) penetration (c) measured at s194 in the open ocean.

4785

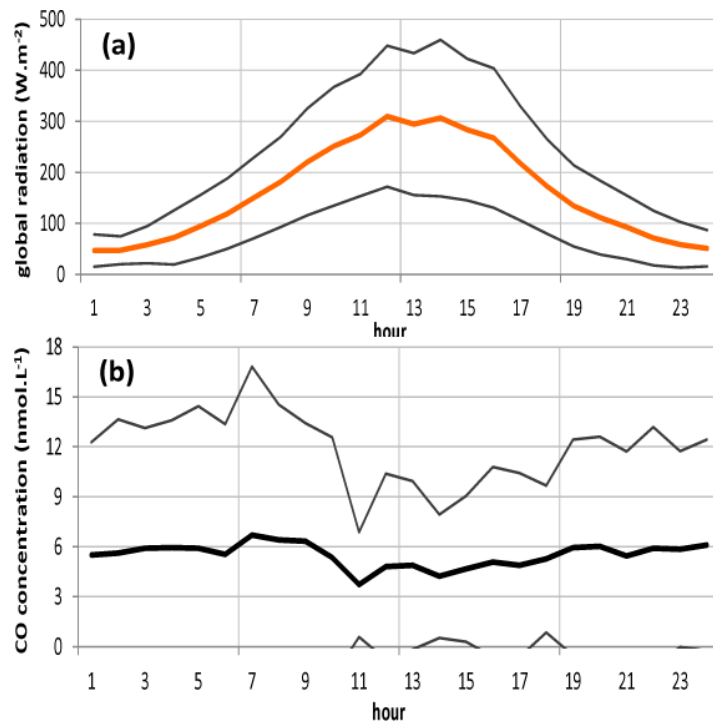


**Fig. 11.** (a) Average diurnal cycle of the solar radiation (W m<sup>-2</sup>) and (b) of CO (nmol l<sup>-1</sup>) over the whole cruise (full solid line), with the standard deviation (light solid line).

4786

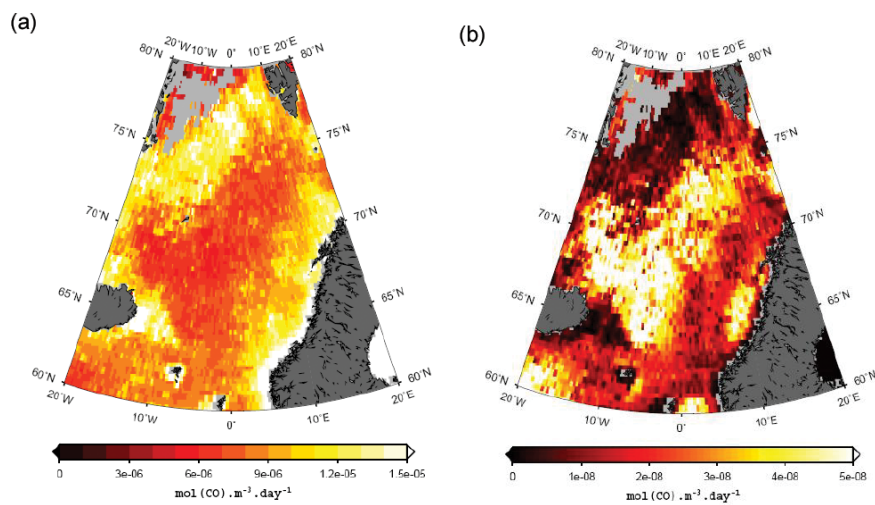


**Fig. 12.** Surface CO production (a) and CO production at a depth of 20 m (b) from Fichot et al. (2010).

4787

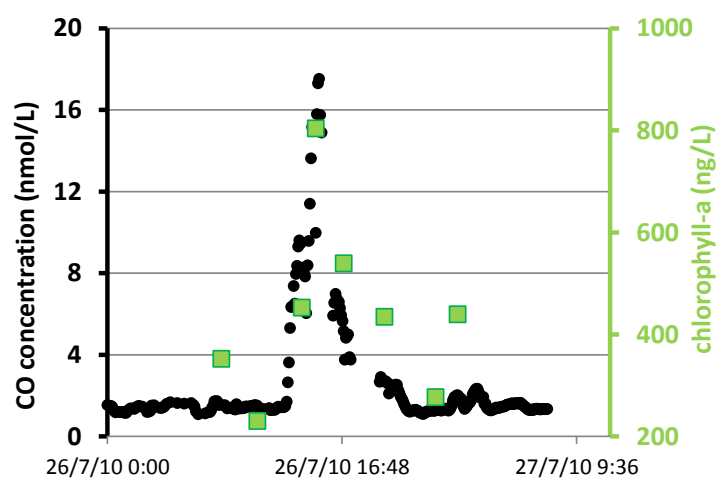


**Fig. 13.** Variability of surface-seawater CO concentration ( $\text{nmol l}^{-1}$ ) combined with chlorophyll a measurements ( $\text{ng l}^{-1}$ ) during the event of 26 July 2010.

4788

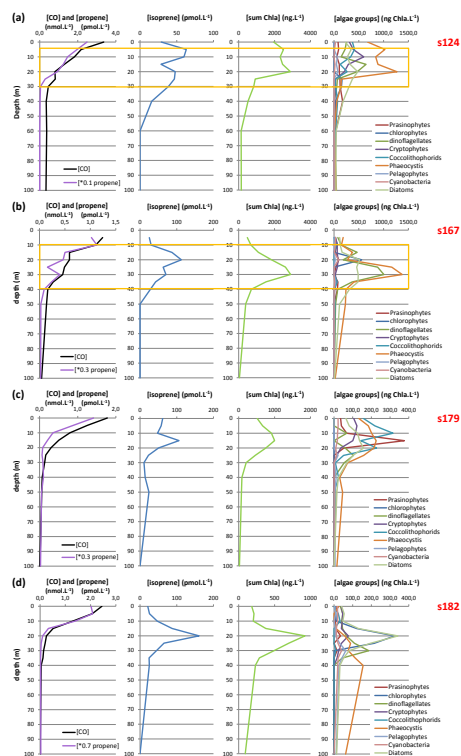


**Fig. 14.** Profiles of CO (nmol l<sup>-1</sup>), propene (values have been multiplied by a factor x to fit in the CO figure, pmol l<sup>-1</sup>), isoprene (pmol l<sup>-1</sup>), chlorophyll a (ng l<sup>-1</sup>) levels and abundances of phytoplankton (ng Chla l<sup>-1</sup>) for stations s124 (a), s167 (b), s179 (c) and s182 (d).

4789

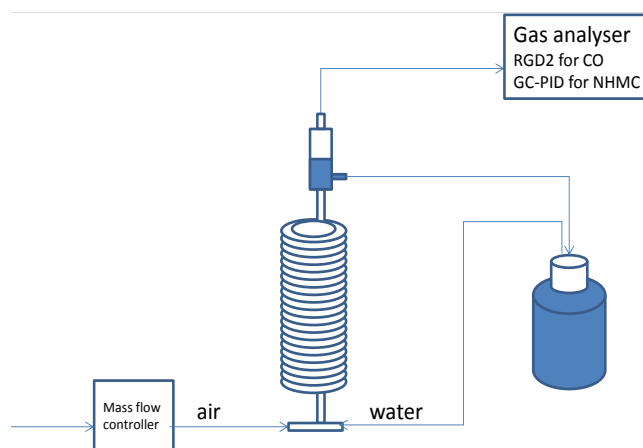


**Fig. A1.** Principle of the closed system.

4790



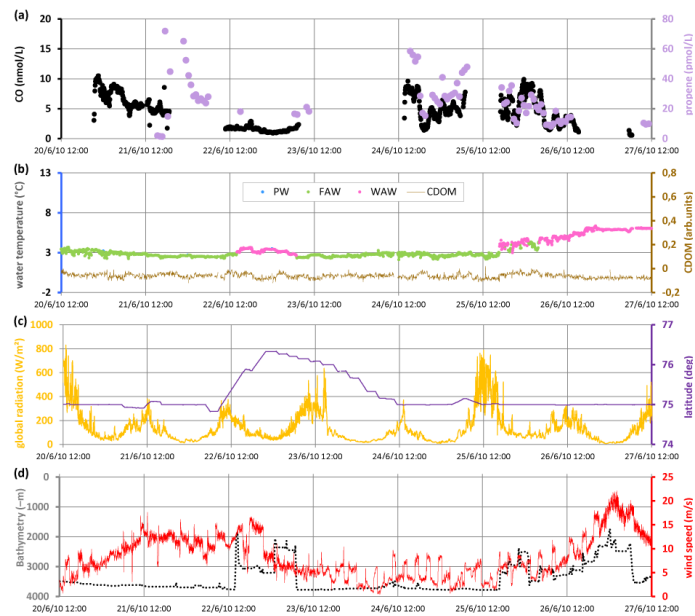


**Fig. C1.** (a) Sea-surface CO ( $\text{nmol l}^{-1}$ ) and propene ( $\text{pmol l}^{-1}$ ) concentrations; (b) water temperature ( $^{\circ}\text{C}$ ), which included the identification of water masses: PW = Polar water, FAW = Fresh Atlantic Water, WAW = Warm Atlantic Water, AW = Atlantic Water with low salinity, and CDOM concentration (ppb); (c) global radiation ( $\text{W m}^{-2}$ ) and latitude (deg); and (d) bathymetry (m) and wind speed ( $\text{m s}^{-1}$ ) for section two.

4791

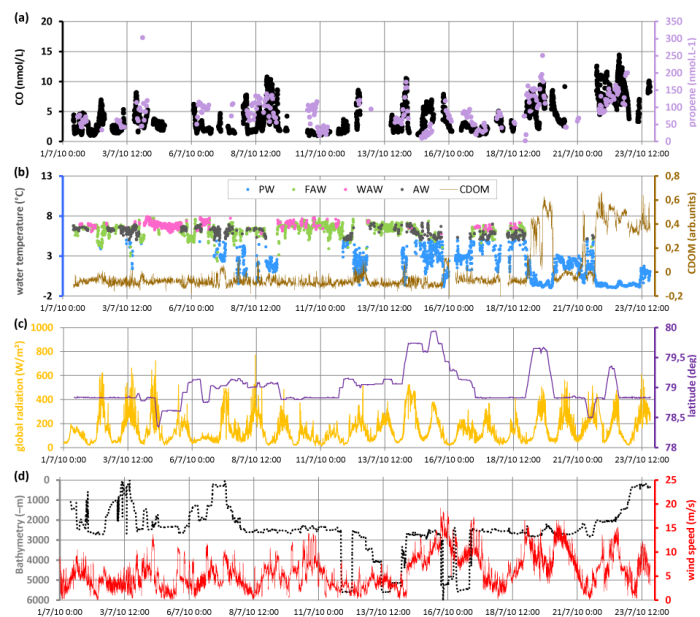


**Fig. C2.** (a) Sea-surface CO ( $\text{nmol l}^{-1}$ ) and propene ( $\text{pmol l}^{-1}$ ) concentrations; (b) water temperature ( $^{\circ}\text{C}$ ), which included the identification of water masses: PW = Polar water, FAW = Fresh Atlantic Water, WAW = Warm Atlantic Water, AW = Atlantic Water with low salinity, and CDOM concentration (ppb); (c) global radiation ( $\text{W m}^{-2}$ ) and latitude (deg); and (d) bathymetry (m) and wind speed ( $\text{m s}^{-1}$ ) for section three.

4792